Symmetry Breaking in Gold−Silica−Gold Multilayer Nanoshells

Ying Hu,[†] Sterling J. Noelck,[†] and Rebekah A. Drezek[†,‡,*]

[†]Department of Bioengineering and [‡]Department of Electrical and Computer Engineering, Rice University, Houston, Texas 77005

ABSTRACT We present a computational study of the plasmonic properties of gold−silica−gold multilayer nanoshells with the core offset from the center. Symmetry breaking, due to the core offset, makes plasmon resonances that are dark in concentric geometries visible. Applying plasmon hybridization theory, we explain the origin of these resonances from the interactions of an admixture of both primitive and multipolar modes between the core and the shell. The interactions introduce a dipole moment into the higher order modes and significantly enhance their coupling efficiency to light. To elucidate the symmetry breaking effect, we link the geometrical asymmetry to the asymmetrical distribution of surface charges and demonstrate illustratively the diminishing multipolar characteristic and increasing dipolar characteristic of the higher order modes. The relative amplitudes of the modes are qualitatively related by visual examination of the dipolar component in the surface charge distributions. Using polarization-dependent surface charge plots, we illustrate two distinct mode configurations despite their spectral similarities. We further demonstrate a trend of increasing absorption relative to scattering as the resonant wavelength red shifts in response to a larger core offset.

KEYWORDS: plasmonics · multilayer nanoshells · symmetry breaking · plasmon hybridization · surface charge distribution

Up to date, symmetry breaking has been investigated in a variety of gold nanostructures from three-dimensional nanoeggs[1] and nanocups[2] to two-dimensional disk/ring,[3,4] two-layer, and planar nanocavities.[5,6] In nanoeggs, where the silica core is off-centered in a silica−gold core−shell nanoshell, both far-field and near-field properties have been studied as functions of the core offset.[1] It was found that a larger offset correlates with larger red shifts in the low-energy plasmon resonant peaks, a stronger near-field enhancement, and a larger absorption-to-scattering ratio at the dipole resonance.[1] The polarization of light only weakly affects the far-field spectrum.[2] However, in nanocups where the gold shell is partially opened up by the offsetting core, the far-field scattering spectrum strongly depends on polarization owing to its anisotropic geometry.[7] As the core further protrudes from the shell, dipole modes gradually weaken and eventually vanish.[1]

Studies of two-dimensional structures have revealed some interesting phenomena. In geometries with reduced symmetry, the highly damped multipolar modes are excited and interact with the dipole mode. Liu and co-workers demonstrated a carefully designed planar geometry in which the narrow quadrupole resonance of the nanobar/nanoslit dimer destructively interferes with the broad dipole mode of the nanobar/nanoslit monomer that is off-centered, leading to a narrow region where light transmission is significantly enhanced; in atomic physics, this is known as electromagnetically enhanced interference (EIT).[5,6] Similarly, Hao et al. reported a nonconcentric ring/disk nanocavity in which the broad dipole mode both constructively and de-

structively interferes with a sharp quadrupole mode. The interaction results in an asymmetrical sharp Fano-type resonance.[3,4] Due to the sharp nature of the Fano resonance, symmetry-breaking geometries have been proposed for nanoscale optical sensing such as high figure-of-merit metamaterial sensors.[5] It has also been found that offset geometries exhibit significantly larger local-field enhancement, making them promising for surface-enhanced spectroscopies.[1−3]

Multilayer nanoshells (MNS) preserve three-dimensional spherical symmetry, as in nanoeggs, but they also exhibit symmetry-breaking patterns similar to ring/disk nanocavities. Theoretical investigations of concentric MNS have been previously reported using various Mie-based approaches.[8−11] It has been found that the addition of a gold core to the gold shell splits the low-energy plasmon resonance of a conventional silica−gold core−shell nanoshell (CNS) into a high-energy
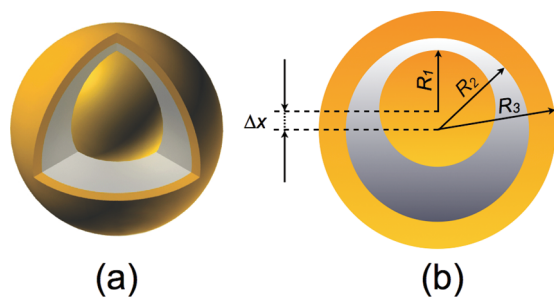
Figure 1. (a) Three-dimensional illustration of a gold—silica—gold multilayer nanoshell with an offset core. (b) Dimensions of an $R_1/R_2/R_3$ gold—silica—gold multilayer nanoshell with core offset Δx.

antibonding mode and a low-energy bonding mode that can be tuned from the visible region into the infrared. The red shift of this mode correlates with intermediate silica layer thickness, which determines the strength of coupling between the core mode and the CNS mode. As the mode red shifts, the MNS becomes relatively more absorbing than scattering at the bonding-mode resonance.[10] An experimental study of MNS has also been published. Xia and co-workers reported the chemical synthesis of sub-100 nm multilayer nanoshells.[12] The silica coating on gold was achieved using a modified Stöber method.[13−16] The final gold layer was coated in a way similar to synthesizing silica—gold core—shell nanoshells.[17,18]

Here we use a computational model to investigate MNS with an offset geometry: the inner gold core is moved away from the center but does not touch the gold shell, as illustrated in Figure 1a. The MNS dimensions are denoted by the radius of each layer, R_1, R_2, and R_3, as well as the core offset, Δx, shown in Figure 1b. We apply plasmon hybridization theory to obtain insight into spectral properties of the MNS. This theory is analogous to molecular orbital theory and describes how the fixed-frequency plasmons of elementary nanostructures hybridize to create more complicated resonances. It has been used to explain the plasmonic properties of structures ranging from concentric nanoshells[19,20] to nanorice[21−24] to nanosphere trimers[25,26] and quadrumers.[25] Some interesting examples of plasmon hybridization applied to nonsymmetrical structures include analyzing the aforementioned nanocups[1,2,7] and nonconcentric ring/disk structures.[3,4]

The far-field properties of MNS were simulated using a finite-element method (FEM) package: COMSOL Multiphysics v3.5a with the RF module. Because the dimensions of the gold core and shell remain unaltered as the location of the core changes, the offset process itself does not require size correction for the dielectric function of gold due to intrinsic effects. It should also be noted that this work does not focus on the spectral width of plasmon resonances, which can be consider-
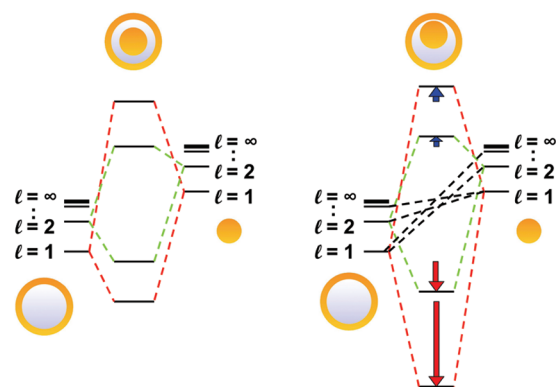

Figure 2. Hybridization diagrams of MNS with concentric (left) and offset (right) geometries. The left panel illustrates the plasmon hybridization diagram for a concentric MNS with interaction between modes having the same angular momentum (energy increases from bottom to top). The right panel displays the nonconcentric MNS case with black lines showing additional interactions and arrows showing the relative red shift and blue shift (not to scale). Only dipole and quadrupolar interactions are shown for clarity.

ably broadened by the surface scattering of electrons in nanostructures.[27−30]

RESULTS AND DISCUSSION

Plasmon Hybridization. An MNS can be modeled as a hybrid between a silica—gold core—shell nanoshell and a solid gold core. We apply plasmon hybridization to explain the optical properties of MNS using these two basic nanostructures. The hybridization diagrams in Figure 2 show, for both the concentric and offset MNS, the interactions between the hybridized modes of the nanoshell and the spherical plasmon modes of the core. For clarity, only the dipolar and quadrupolar interactions are shown. The antibonding modes from the nanoshell are not shown because they are higher energy and have only very weak interactions with the core mode. The left panel of Figure 2 shows the hybridization diagram for the concentric MNS where the modes of different angular momenta are forbidden from interacting. Like the hybridization between the inner and outer layers of a nanoshell, there are two modes for each interaction: a low-energy bonding mode and a higher energy antibonding mode. This can be seen in the left panel of Figure 2 for the dipole—dipole ($l = 1$) and quadrupole—quadrupole ($l = 2$) interaction. For the nonconcentric case, the selection rules for interaction are relaxed, allowing modes of different orders to mix. As depicted in the right panel of Figure 2, the dipole mode ($l = 1$) of the core can now interact with not only the dipole mode ($l = 1$) of the shell but also the quadrupole and higher order modes ($l = 2, 3, etc.$) of the shell. Additionally, the quadrupole ($l = 2$) of the shell can now interact with the dipole ($l = 1$) of the core, bringing in the dipole moment into the quadrupole mode.

The hybridization between different modes on the core and the shell also results in red shifts of the hybrid-

ized bonding modes of MNS. The lower order modes are red-shifted as they become repelled by the interaction with higher order modes. As shown in the right panel of Figure 2, this yields a shift for the predominately dipole−dipole hybridized modes that is larger than for the quadrupolar−quadrupolar hybridized modes, and so on. In addition to a red shift of the bonding modes, the antibonding hybridized modes are slightly blue-shifted. This leads to a very asymmetrical splitting of the hybridized energy modes. Such asymmetrical splitting is seen in other nanostructures as the symmetry is broken,[2,4,31] as well as in nanoparticle dimers.[32,33] The degree of the shift is determined by the strength of the interactions between the different modes. As the gold core is offset more and approaches the gold nanoshell, the plasmons of the core interact more strongly with plasmons of the shell. These increasing interactions lead to stronger mixing between the different modes, creating a greater shift from the concentric MNS interactions.

Symmetry Breaking in MNS with Different Geometries. As seen in the work on concentric multilayer nanoshells, changing the ratio of the core, silica layer, and the outer layer allows tuning of the plasmon resonance.[10] This same effect is seen in offset multilayer nanoshells, as well. Figures 3 and 4 show the extinction spectra of the offset MNS with two different $R_1/R_2/R_3$ ratios as well as different outer radii R_3. Figure 3 shows R10/15/25 nm MNS in water with various core offsets. The black stars from the Mie calculation agree very well with the black curve from the FEM calculation of a concentric geometry. Two distinct plasmon resonant peaks can be observed in the concentric spectrum. The high-energy peak around 530 nm is the antibonding mode of the dipole−dipole interaction between the shell and the core along with other higher order modes. The interband transitions of gold lead to a pronounced broadening and damping of all modes in this region.[34−36] The low-energy peak at 643 nm is the bonding mode of the dipolar interaction. Quadrupole modes are not excited as the particle lies in the quasi-static region. When the symmetry is reduced and the mode selection rule for hybridization is relaxed, modes of different angular momenta start to interact.[1,2,31] Among the offset spectra, one can immediately observe a red shift of the dipolar bonding mode. The fact that the dipole of the core is allowed to interact with the quadrupole of the shell and *vice versa* shifts the bonding mode to a lower energy. The blue shift of the antibonding mode, however, is too small to be visualized in the spectrum. In addition to the red shift of the bonding modes and blue shift of the antibonding modes, hybridization results in the appearance of dark modes that were only weakly excited or not excited at all in the concentric MNS. For instance, one can observe the emergence of a new peak at about 592 nm. This peak is likely to be the bonding mode of the quadrupole−quadrupole interaction between the
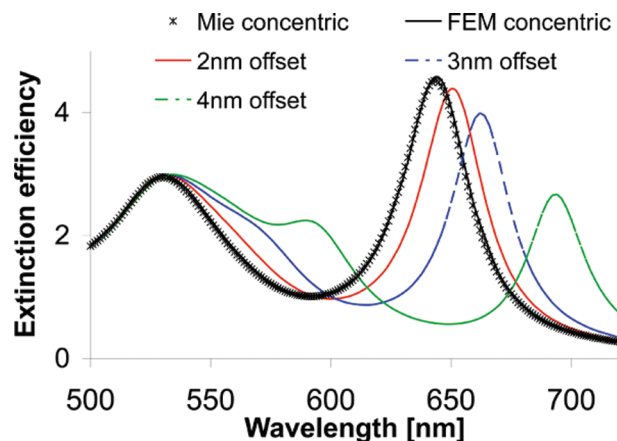

Figure 3. Extinction spectra of R10/15/25 nm MNS in water with various core offsets. Core offsets in *y*; incident light linearly polarized in *x* and propagates in *z*.

shell and the core (noted by $l = 2$ in the hybridization diagram). This mode can be directly excited because the interaction between the quadrupolar and dipole modes introduces a small overall dipole moment in the plasmon. This mode is not excitable in the concentric case because of the lack of the dipole moment in the quadrupole−quadrupole interaction.

Although interesting in nature, the quadrupole peak is still not very well-defined at the largest offset we calculated. In Figure 4, we demonstrate the spectra of a larger MNS: R30/40/50 nm in water with a different $R_1/R_2/R_3$ ratio (3/4/5 instead of 2/3/5). The particle lies outside the quasistatic region and can provide opportunities to observe sharp higher order modes. As shown in Figure 4, good agreement was obtained between Mie and FEM calculations on the concentric geometry. The relatively large size of the MNS and limitations from the meshing and scattering boundary condition in COMSOL v3.5a may account for the ∼6% discrepancy on the peak intensity at 890 nm.[37] For clarity, each resonant peak is labeled with a numerical value associated with its mode (*i.e.*, 1 for dipole, 2 for quadrupole, *etc.*), followed by a letter denoting the core offset of that spectrum.
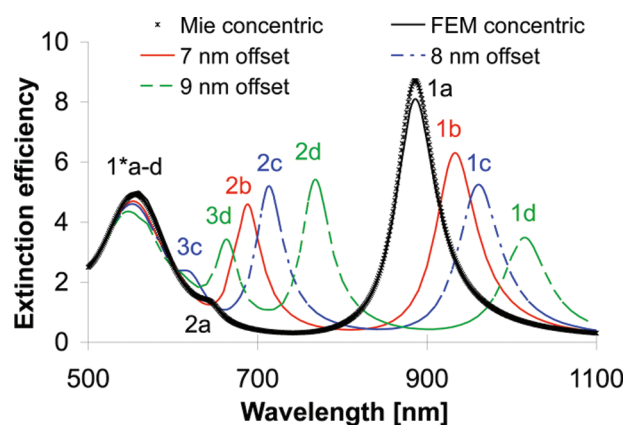

Figure 4. Extinction spectra of R30/40/50 nm MNS in water with various core offsets. Core offsets in *y*; incident light linearly polarized in *x* and propagates in *z*.

In the concentric spectrum, in addition to the dipolar modes at 1a and 1*a, a slight quadrupolar peak can be observed at 2a. The excitation of this mode is attributed to the retardation effect as the particle size is comparable to the excitation wavelength. Its small amplitude reflects a lack of the dipole moment. More specifically, the amplitude of the extinction peak is directly proportional to the square of the dipole moment. When the symmetry is reduced, as shown in the 7 nm offset spectrum (red), the dipolar bonding mode is redshifted from 886 to 934 nm (1a to 1b) and the quadrupolar bonding mode is shifted from ~644 to 688 nm (2a to 2b). While the peak intensity of 1b is decreased, that of 2b is significantly enhanced. The enhancement at 2b is due to the dipole−quadrupole interaction that adds a dipolar component into the quadrupole mode. Likewise, the interaction between the dipole of the core/shell and higher order modes of the core/shell introduces dark characteristics of the multipolar modes into 1b and causes its amplitude to decrease.

From a macroscopic perspective, the *f-sum law* can be used to interpret the relative change of the peak amplitude at each plasmon mode.[38,39] In the MNS system, where the number of oscillating electrons is fixed, the convolution of the amplitudes of plasmon resonances with their energy levels remains a constant. This does not, however, indicate that an increase in one peak necessarily causes a decrease in another peak. In the 7 nm offset spectrum, nevertheless, the significant gain at the high-energy quadrupolar mode demands that the dipolar mode be both down shifted in energy and decreased in amplitude.

As the core continuously moves away from the center, more modes that are completely dark in the concentric spectrum start to emerge. In the 8 nm (blue) and 9 nm (green) offset spectra, the emergence of the 3c mode at ~620 nm and the 3d mode at 664 nm is the octupole mode excited with added dipole components. As previously described by the *f-sum law*, the introduction of this new octupole mode results in a decrease in amplitude of the dipole mode at 1c and 1d.

Surface Charge Distribution and the Polarization Effect. While hybridization theory qualitatively explains the plasmon resonances of MNS, it does not provide information regarding charge distributions on metal−dielectric interfaces at each resonant mode. Furthermore, it does not describe the relative amplitude of each peak nor the polarization effect on the spectrum. Therefore, we supplement the hybridization analysis with surface charge distributions at the outer and inner layers of the gold shell as well as the surface of the gold core at resonant wavelengths. We examine both spectral properties and charge distributions of the MNS when the incident light is axially polarized with respect to the core offset and when it is transversely polarized.

Figure 5 shows the extinction spectra of the R30/40/50 nm MNS with a 9 nm offset core at two different
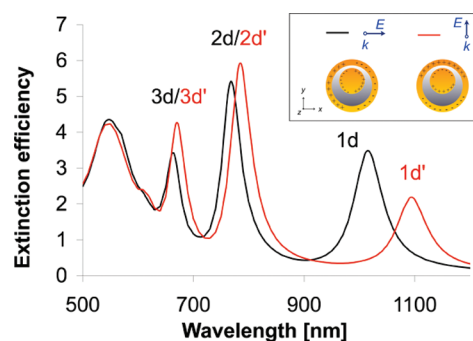

Figure 5. Extinction spectrum of the R30/40/50 nm MNS in water with 9 nm core offset. Black, incident light is transversely polarized with respect to the offset; red, incident light is axially polarized along the offset.

polarizations. The dipole, quadrupole, and octupole resonances can be clearly recognized, as described in previous sections. To facilitate the analysis, we denote these modes in the following fashion: dipole modes 1d (transverse) and 1d′ (axial), quadrupole modes 2d (transverse) and 2d′ (axial), and octupole modes 3d (transverse) and 3d′ (axial). One can observe that the two spectra have very similar shapes, indicating minimal impact from polarization. It is worth noting that reported in the literature are three-dimensional nanoparticles whose plasmon resonances do not largely depend on the polarization, such as nanoeggs,[2] and nanoparticles whose spectra bear distinct polarization-dependent characteristics, such as nanocups.[7] We conjecture that, since the offset MNS bear more resemblance to the nanoegg structure, the spectra should be largely polarization independent. One can observe in the axial spectrum slight red shifts in the bonding modes: from 1016 to 1094 nm for the dipole mode, 768 to 785 nm for the quadrupole mode, and 664 to 670 nm for the octupole mode. The red shift implies a stronger interaction between modes with different angular momenta when the light is axially polarized along the small gap between the core and the shell. One can also observe that 1d′ has the largest red shift, whereas 3d′ has the least. This is in agreement with the plasmon hybridization theory shown in Figure 2. In addition, the quadrupole and octupole peaks in the axially polarized spectrum (2d′ and 3d′) appear to be higher than those in the transversely polarized spectrum (2d and 3d), possibly owing to the stronger interaction. In both spectra, the quadrupole peaks (2d and 2d′) appear to be higher than the octupole peaks (3d and 3d′). We will now explore these observations from the surface charge perspective. To calculate the surface charge, Gauss's law was applied to metal−dielectric interfaces. The phase of the solution was swept to find the correct distribution that corresponds to the maximal surface charge density. The extinction spectrum was calculated for the geometry in which the core offset and light polarization were (1) in orthogonal directions (transverse) and (2) along the same direction (axial).

Figure 6 shows the charge distribution on metal−dielectric interfaces for plasmon modes in the transverse spectrum. Side and top views (left and right panel) are provided. The color scales (not shown) on each surface are different for better illustration. Three relevant observations can be made. First, the distributions at 3d, 2d, and 1d resemble octupole, quadrupole, and dipole-like characteristics, respectively. Opposite charges are found on the surface along the *E* field direction in which light is polarized. At each resonance, the charge distribution exhibits an alternating half-ring shape stacked from the top to the bottom of the particle. The pattern is consistent with the predictions we made using plasmon hybridization theory. Second, one observes that the charge polarity is the same along the inner and outer surfaces of the gold shell. This corresponds to the bonding-mode configuration of the shell and indicates that the core is, in fact, interacting with the bonding mode of the shell. Further, the charge polarity on the inner core is oppositely aligned with the outer shell. This also corresponds to the low-energy configuration (bonding) of the MNS and indicates that the plasmon resonance is the low-energy bonding mode from the core−shell interaction. Lastly, the octupole, quadrupole, and dipole distributions appear spatially distorted. The nature of the spatial asymmetry indicates that the hybridized modes are composed of a mixture of modes with different angular momenta. For instance, a perfect quadrupole mode would appear evenly and symmetrically distributed along each quadrant of the spherical surface. The fact that the distribution is skewed, as can be seen in the left panel of Figure 6, is caused by the admixture of a dipole component polarized along the horizontal direction. Since the plasmon resonant peak amplitude is directly proportional to the square of the dipole moment, the quadrupole and octupole modes are enhanced due to the introduction of the dipole interaction and the added dipole components, whereas the dipole mode will have a lower peak owing to the interaction with the multipolar modes and a reduction of the dipole component. Additionally, the degree of asymmetry of the charge distributions for the multipolar modes directly implies the amount of the dipole moment that has been added to the mode. The 2d mode appears to be more asymmetrical in a quadrupole sense than 3d in an octupole sense, suggesting that 2d has a larger dipole moment. This is better revealed in the spectrum in Figure 5, where 2d has a higher amplitude than 3d.

When the incident light is axially polarized, the surface charge distributions exhibit distinct characteristics despite spectral similarities to the transverse polarization case. As shown in the right
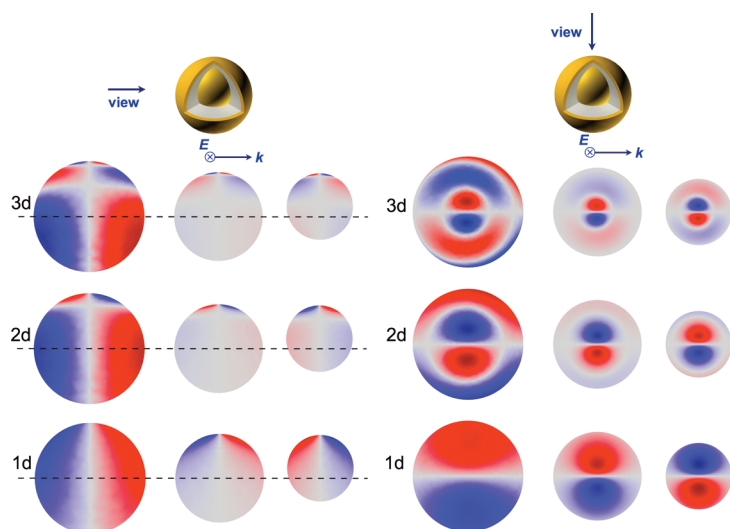

Figure 6. Side (left) and top (right) views of the surface charge plot of R30/40/50 nm MNS with 9 nm core offset at various hybridized plasmon peaks as the incident light is transversely polarized with respect to the offset. The three columns correspond to the outer gold shell (left), inner gold shell (middle), and inner gold core (right) layers. Red, positive charges; blue, negative charges. Horizontal dashed lines in the left panel mark the center location with respect to the core offset.

panel of Figure 7, the octupole and quadrupole distributions appear as whole rings instead of half rings across the entire particle. A larger dipole moment can be recognized in 3d′ and 2d′ as the charge distributions become more dipole-like. Meanwhile, the dipolar distributions in 1d′ also appear distorted, indicating a large multipolar interaction, which attenuates and red shifts the resonant peak. Because the overall degree of asymmetry is larger in Figure 7 than in Figure 6, we conclude that the mode hybridization due to symmetry breaking is stronger when the light is axially polarized. This explains the overall red shift from 1d, 2d, and 3d to
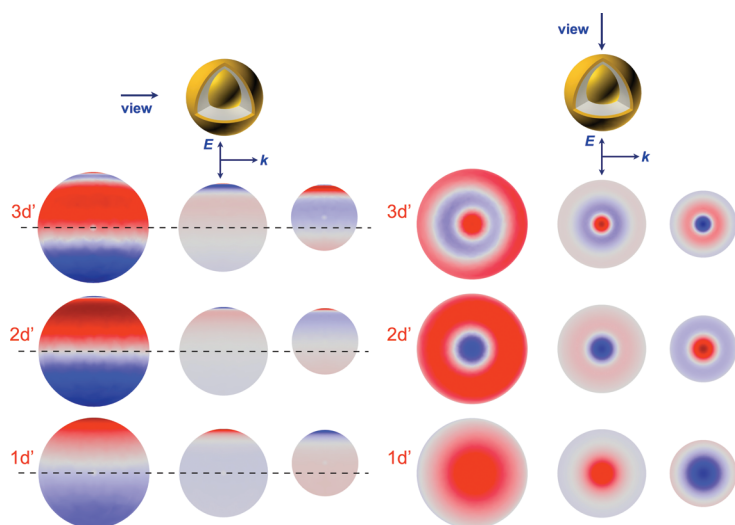

Figure 7. Side (left) and top (right) views of the surface charge plot of R30/40/50 nm MNS with 9 nm core offset at various hybridized plasmon peaks as the incident light is axially polarized along the offset. The three columns correspond to the outer gold shell (left), inner gold shell (middle), and inner gold core (right) surfaces. Red, positive charges; blue, negative charges. Horizontal dashed lines in the left panel mark the center location with respect to the core offset.
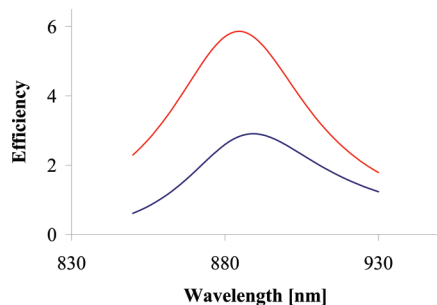
Figure 8. Mie-based calculation of the absorption (red) and scattering (blue) spectra of the concentric R30/40/50 nm MNS in water near the dipolar resonance.

1d′, 2d′, and 3d′ and also the higher amplitudes at 2d′, 3d′ *versus* 2d, 3d and the lower amplitude at 1d′ *versus* 1d, as previously described. It is worth noting that, due to the relatively large size of the particle (100 nm), the retardation from the propagating electromagnetic wave comes into play. For instance, in the right panels of Figures 6 and 7, the left−right asymmetry of the charge distribution for the octupole modes reveals this retardation effect. Waves travel in slightly different phase across the particle along the direction of the propagation (indicated by the *k* vector), which yields a slightly asymmetric charge distribution.

When MNS are excited by circularly polarized light (see Supporting Information), the surface charge distribution is a hybrid between the two types described above. The distributions not only appear distorted along the direction of the core offset but also become skewed around the spherical surface. The basic analysis, however, falls in the discussions for the axial and transverse polarizations.

Absorption Relative to Scattering. In concentric MNS, an increase of the gold core in an otherwise fixed geometry red shifts the dipolar bonding mode and renders the particle more absorbing than scattering at the plasmon resonance.[10] It is thus of interest to investigate how the absorption of MNS changes with respect to scattering as a function of the core offset. We chose to focus on the dipolar and quadrupolar peaks and compare the absorption and scattering components of overall extinction. It is important to note that the wavelengths of peak values for absorption and scattering are slightly offset from each other. This is manifested not just in the FEM calculations of offset geometries but also in the Mie-based calculations of concentric geometries. The R30/40/50 nm MNS with a 9 nm offset and excited by transversely polarized light has an extinction peak at 886 nm, while the absorption peak is at 885 nm and the scattering peak at 889 nm. The offset is noticeable in Figure 8. The offset value, however, is small enough so the actual scattering and absorption values do not change very much. For consistency, we used the absorption and scattering values at the peak extinction wavelength for the comparisons in Figure 9a,b.
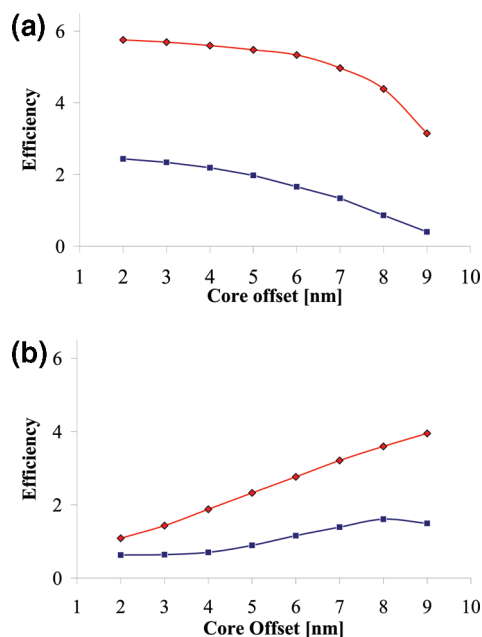

Figure 9. FEM calculation of the absorption (red) and scattering (blue) efficiency of the R30/40/50 nm MNS with a variable core offset in water (a) at the dipolar resonance and (b) at the quadrupolar resonance. Incident light transversely polarized.

From Figure 9a, it is clear that both scattering and absorption decrease with increasing offset, and the particle becomes more absorbing relative to scattering at the dipole peak. The scattering component steadily decreases and becomes almost insignificant at large offsets. The quadrupolar peak, shown in Figure 9b, is more complicated as the scattering first increases and then decreases after the 8 nm offset. Although with the decreasing scattering, the overall extinction continues to increase due to the rapidly growing absorption. The stronger absorption of the metal is mainly caused by a larger field confinement within a smaller volume (*i.e.*, the reducing gap between the core and the shell). These general trends are also seen in a R20/30/50 nm MNS (see Supporting Information). Overall, our results show a general trend toward a larger absorption component in the extinction peak as the core offset increases.

CONCLUSION

In this paper, we used plasmon hybridization theory and demonstrated that an offset of the core in an MNS allows interactions between plasmon resonances of different angular momenta. The mixing of modes allowed by the broken symmetry introduces a dipolar characteristic into higher order multipolar modes and makes them visible in the extinction spectra. We presented qualitatively in a hybridization diagram and quantitatively in the FEM calculations red shifts of the bonding plasmon modes as well as the emergence of the multipolar modes in the offset MNS. While polariza-

tion has little effect on the extinction spectra, we demonstrated that different polarizations create distinctly different surface charge distributions. We decomposed the extinction spectra into scattering and absorption and found that MNS tend to have a larger absorption component relative to scattering as the core offset increases. We postulate that offset MNS with larger dimensions will exhibit more interesting multiwavelength

plasmon resonances that are associated with even higher order modes. Assuming methods for large-scale synthesis can be developed, such particles may become valuable for multiplexed imaging. The distinctive spectral properties of MNS and their sensitivity to the core offset can also be harnessed to provide proof-of-concept studies for tracking intracellular movements of vessels and capsules that contain gold nanoparticles.

METHODS

For the FEM simulations, gold properties were obtained from Johnson and Christy.[40] The dielectric constant of silica was set to 2.04, and that for water to 1.33. The surrounding medium of MNS was water. Simulations were performed in COMSOL Multiphysics v3.5a. The simulation space and perfectly matched layer thickness were adjusted until agreement was obtained between the FEM and Mie-based calculations.[10]

For optical spectra, the scattering efficiency was calculated by integrating the normalized E field around a far-field transform boundary enclosing the MNS. The absorption efficiency was calculated by summing time-average resistive heating on the inner gold core and other gold shell. For surface charge plots, Gauss's law was applied:

$$\varepsilon_0 \iint \vec{E}\cdot\vec{n}\,\mathrm{d}S = \iint \sigma \mathrm{d}S$$

The gradient operation was realized by implementing the *up* and *down* operators to the metal−dielectric interfaces in COMSOL.

Mie calculations were implemented in an in-house Matlab code written for simulating light scattering from concentric spheres with arbitrary number of layers.[10] The dielectric function of gold was kept the same as the one used in FEM calculations, so were other parameters such as the refractive index of silica and water. The Mie code has been previously validated against literature results.[10,41]

REFERENCES AND NOTES

1. Knight, M. W.; Halas, N. J. Nanoshells to Nanoeggs to Nanocups: Optical Properties of Reduced Symmetry Core−Shell Nanoparticles Beyond the Quasistatic Limit. *New J. Phys.* **2008**, *10*, 105006.
2. Wang, H.; Wu, Y. P.; Lassiter, B.; Nehl, C. L.; Hafner, J. H.; Nordlander, P.; Halas, N. J. Symmetry Breaking in Individual Plasmonic Nanoparticles. *Proc. Natl. Acad. Sci. U.S.A.* **2006**, *103*, 10856–10860.
3. Hao, F.; Nordlander, P.; Sonnefraud, Y.; Van Dorpe, P.; Maier, S. A. Tunability of Subradiant Dipolar and Fano-Type Plasmon Resonances in Metallic Ring/Disk Cavities: Implications for Nanoscale Optical Sensing. *ACS Nano* **2009**, *3*, 643–652.
4. Hao, F.; Sonnefraud, Y.; Van Dorpe, P.; Maier, S. A.; Halas, N. J.; Nordlander, P. Symmetry Breaking in Plasmonic Nanocavities: Subradiant LSPR Sensing and a Tunable Fano Resonance. *Nano Lett.* **2008**, *8*, 3983–3988.
5. Liu, N.; Weiss, T.; Mesch, M.; Langguth, L.; Eigenthaler, U.; Hirscher, M.; Sonnefraud, Y.; Giessen, H. Planar Metamaterial Analogue of Electromagnetically Induced Transparency for Plasmonic Sensing. *Nano Lett.* **2009**, DOI: 10.1021/nl902621d.
6. Liu, N.; Langguth, L.; Weiss, T.; Kastel, J.; Fleischhauer, M.; Pfau, T.; Giessen, H. Plasmonic Analogue of Electromagnetically Induced Transparency at the Drude Damping Limit. *Nat. Mater.* **2009**, *8*, 758–762.
7. Lassiter, J. B.; Knight, M. W.; Mirin, N. A.; Halas, N. J. Reshaping the Plasmonic Properties of an Individual Nanoparticle. *Nano Lett.* **2009**, *9*, 4326–4332.
8. Chen, K.; Liu, Y.; Ameer, G.; Backman, V. Optimal Design of Structured Nanospheres for Ultrasharp Light-Scattering Resonances as Molecular Imaging Multilabels. *J. Biomed. Opt.* **2005**, *10*, 024005.
9. Khlebtsov, B.; Khlebtsov, N. Ultrasharp Light-Scattering Resonances of Structured Nanospheres: Effects of Size-Dependent Dielectric Functions. *J. Biomed. Opt.* **2006**, *11*, 044002.
10. Hu, Y.; Fleming, R. C.; Drezek, R. A. Optical Properties of Gold−Silica−Gold Multilayer Nanoshells. *Opt. Express* **2008**, *16*, 19579–19591.
11. Wu, D. J.; Liu, X. J. Tunable Near-Infrared Optical Properties of Three-Layered Gold−Silica−Gold Nanoparticles. *Appl. Phys. B* **2009**, *97*, 193–197.
12. Xia, X. H.; Liu, Y.; Backman, V.; Ameer, G. A. Engineering Sub-100 nm Multi-layer Nanoshells. *Nanotechnology* **2006**, *17*, 5435–5440.
13. Graf, C.; Vossen, D. L. J.; Imhof, A.; van Blaaderen, A. A General Method to Coat Colloidal Particles with Silica. *Langmuir* **2003**, *19*, 6693–6700.
14. Kobayashi, Y.; Katakami, H.; Mine, E.; Nagao, D.; Konno, M.; Liz-Marzan, L. M. Silica Coating of Silver Nanoparticles Using a Modified Stöber Method. *J. Colloid Interface Sci.* **2005**, *283*, 392–396.
15. Lee, H. B.; Yoo, Y. M.; Han, Y. H. Characteristic Optical Properties and Synthesis of Gold−Silica Core−Shell Colloids. *Scripta Mater.* **2006**, *55*, 1127–1129.
16. LizMarzan, L. M.; Giersig, M.; Mulvaney, P. Synthesis of Nanosized Gold−Silica Core−Shell Particles. *Langmuir* **1996**, *12*, 4329–4335.
17. Westcott, S. L.; Oldenburg, S. J.; Lee, T. R.; Halas, N. J. Formation and Adsorption of Clusters of Gold Nanoparticles onto Functionalized Silica Nanoparticle Surfaces. *Langmuir* **1998**, *14*, 5396–5401.
18. Oldenburg, S. J.; Averitt, R. D.; Westcott, S. L.; Halas, N. J. Nanoengineering of Optical Resonances. *Chem. Phys. Lett.* **1998**, *288*, 243–247.
19. Prodan, E.; Radloff, C.; Halas, N. J.; Nordlander, P. A Hybridization Model for the Plasmon Response of Complex Nanostructures. *Science* **2003**, *302*, 419–422.
20. Radloff, C.; Halas, N. J. Plasmonic Properties of Concentric Nanoshells. *Nano Lett.* **2004**, *4*, 1323–1327.
21. Sealy, C. Nanorice Combines Best of Both Worlds. *Nano Today* **2006**, *1*, 13.

22. Srivastava, D.; Lee, I. Nanorice and Nanospears from Polymer Nanospheres. *Adv. Mater.* **2006**, *18*, 2471–2475.

23. Wang, H.; Brandl, D. W.; Le, F.; Nordlander, P.; Halas, N. J. Nanorice: A Hybrid Plasmonic Nanostructure. *Nano Lett.* **2006**, *6*, 827–832.

24. Wiley, B. J.; Chen, Y. C.; McLellan, J. M.; Xiong, Y. J.; Li, Z. Y.; Ginger, D.; Xia, Y. N. Synthesis and Optical Properties of Silver Nanobars and Nanorice. *Nano Lett.* **2007**, *7*, 1032–1036.

25. Brandl, D. W.; Mirin, N. A.; Nordlander, P. Plasmon Modes of Nanosphere Trimers and Quadrumers. *J. Phys. Chem. B* **2006**, *110*, 12302–12310.

26. Jain, P. K.; El-Sayed, M. A. Surface Plasmon Coupling and Its Universal Size Scaling in Metal Nanostructures of Complex Geometry: Elongated Particle Pairs and Nanosphere Trimers. *J. Phys. Chem. C* **2008**, *112*, 4954–4960.

27. Berciaud, S.; Cognet, L.; Tamarat, P.; Lounis, B. Observation of Intrinsic Size Effects in the Optical Response of Individual Gold Nanoparticles. *Nano Lett.* **2005**, *5*, 515–518.

28. Kreibig, U.; Vollmer, M. *Optical Properties of Metal Clusters*; Springer: New York, 1995.

29. Moroz, A. Electron Mean Free Path in a Spherical Shell Geometry. *J. Phys. Chem. C* **2008**, *112*, 10641–10652.

30. Nehl, C. L.; Grady, N. K.; Goodrich, G. P.; Tam, F.; Halas, N. J.; Hafner, J. H. Scattering Spectra of Single Gold Nanoshells. *Nano Lett.* **2004**, *4*, 2355–2359.

31. Wu, Y. P.; Nordlander, P. Plasmon Hybridization in Nanoshells with a Nonconcentric Core. *J. Chem. Phys.* **2006**, *125*, 124708.

32. Lassiter, J. B.; Aizpurua, J.; Hernandez, L. I.; Brandl, D. W.; Romero, I.; Lal, S.; Hafner, J. H.; Nordlander, P.; Halas, N. J. Close Encounters between Two Nanoshells. *Nano Lett.* **2008**, *8*, 1212–1218.

33. Nordlander, P.; Oubre, C.; Prodan, E.; Li, K.; Stockman, M. I. Plasmon Hybridization in Nanoparticle Dimers. *Nano Lett.* **2004**, *4*, 899–903.

34. Hao, F.; Nordlander, P. Efficient Dielectric Function for FDTD Simulation of the Optical Properties of Silver and Gold Nanoparticles. *Chem. Phys. Lett.* **2007**, *446*, 115–118.

35. Perner, M.; Bost, P.; Lemmer, U.; vonPlessen, G.; Feldmann, J.; Becker, U.; Mennig, M.; Schmitt, M.; Schmidt, H. Optically Induced Damping of the Surface Plasmon Resonance in Gold Colloids. *Phys. Rev. Lett.* **1997**, *78*, 2192–2195.

36. Pinchuk, A.; Kreibig, U.; Hilger, A. Optical Properties of Metallic Nanoparticles: Influence of Interface Effects and Interband Transitions. *Surf. Sci.* **2004**, *557*, 269–280.

37. Khoury, C. G.; Norton, S. J.; Vo-Dinh, T. Plasmonics of 3-D Nanoshell Dimers Using Multipole Expansion and Finite Element Method. *ACS Nano* **2009**, *3*, 2776–2788.

38. Nozieres, P.; Pines, D. Electron Interaction in Solids—General Formulation. *Phys. Rev.* **1958**, *109*, 741–761.

39. Mahan, G. D. *Many-Particle Physics*; Springer: New York, 1990.

40. Johnson, P. B.; Christy, R. W. Optical Constants of the Noble Metals. *Phys. Rev. B* **1972**, *6*, 4370–4379.

41. Bohren, C. F.; Huffman, D. R. *Absorption and Scattering of Light by Small Particles*; Wiley-VCH: Weinheim, Germany, 2004.